JCTC Journal of Chemical Theory and Computation

ARTICLE

pubs.acs.org/JCTC

A Simple Mechanism Underlying the Effect of Protecting Osmolytes on Protein Folding

G. Saladino,[†] M. Marenchino,[‡] S. Pieraccini,[†,§] R. Campos-Olivas,[‡] M. Sironi,[*,†,§,∥] and F. L. Gervasio[*,‡]

[†]Dipartimento di Chimica Fisica ed Elettrochimica, Universita' degli Studi di Milano, Via Golgi 19, 20133 Milano, Italy

[‡]Structural Biology and Biocomputing Programme, Spanish National Cancer Research Centre (CNIO), c/Melchor Fernandez Almagro 3, 28029, Madrid, Spain

[§]INSTM Research Unit, Via Golgi 19, 20133 Milano, Italy

[∥]Institute of Molecular Science and Technology, Via Golgi 19, 20133 Milano

Supporting Information

ABSTRACT: Osmolytes are small organic compounds that confer to the cell an enhanced adaptability to external conditions. Many osmolytes not only protect the cell from osmotic stress but also stabilize the native structure of proteins. While simplified models able to predict changes to protein stability are available, a general physicochemical explanation of the underlying microscopic mechanism is still missing. Here, we address this issue by performing very long all-atom MD simulations, free energy calculations, and experiments on a well-characterized mini-protein, the villin headpiece. Comparisons between the folding free energy landscapes in pure water and osmolyte solutions, together with experimental validation by means of circular dichroism, unfolding experiments, and NMR, led us to formulate a simple hypothesis for the protecting mechanism. Taken together, our results support a novel mechanistic explanation according to which the main driving force behind native state protection is a change in the solvent rotational diffusion.

INTRODUCTION

Severe environmental conditions, such as extreme temperatures, high osmotic pressure, or high concentrations of urea tend to cause cellular water stress. Many organisms have evolved to respond to these conditions regulating the level of small organic compounds, called osmolytes.[1] Osmolytes have been observed in a wide range of organisms[2] and have been found to accumulate in some species able to survive under harsh conditions,[3,4] such as the so-called "resurrection plants", able to survive under severe drought.[5] In addition to their ability to control cell water loss or gain,[6−8] some osmolytes are also able to stabilize the native fold of proteins.[9] Bolen and co-workers carefully characterized osmolyte-induced thermotolerance,[10,11] due to the alteration of folded−unfolded equilibria. They also demonstrated that trimethylamine N-oxide (TMAO)[11] can fold natively unfolded proteins. Despite the wide variety of proteins in living organisms, only a few, generally interchangeable,[12] osmolyte molecules exist,[1,13] suggesting a universal underlying mechanism. Contrasting theories have been proposed involving either direct[14,15] or indirect interactions with proteins,[16,17] with the latter one recently prevailing due to the observed exclusion of osmolytes, with the exception of the denaturing urea,[18] from the protein surface, a phenomenon coined the "osmophobic effect".[19] Recently, we used simulations and free energy methods to study the effect of the osmolyte glycine betaine (GB) on a small β-hairpin peptide, observing the expected increased stability of the native fold.[20,21] Nevertheless, a simple yet universal explanation of the microscopic mechanism of osmoprotection has not been found. In the search for such a general explanation, here, we combine simulations and experiments to study the effect of osmolytes on a more realistic and well-characterized mini-protein, the human villin headpiece C-terminal helical subdomain (HP35).[22] HP35 has a well-defined secondary and tertiary structure and is one of the smallest peptides that folds cooperatively.[23] It has been the subject of several computational[24,25] and experimental[26−29] studies. In the following, the effect of two different osmoprotectants and urea on the folding of HP35 were investigated using 1.5-μs-long unbiased all-atoms MD simulations and massive bias exchange molecular dynamics simulations (BEMD),[30] as well as calorimetry, circular dichroism (CD), and NMR experiments. The experimentally validated free energies, together with a careful structural analysis, allowed us to outline a clear and simple picture of the osmolyte protecting mechanism.

MATERIALS AND METHODS

The HP35 structure was retrieved from the Protein Data Bank (PDB code: 1UNC).[22] The protein was solvated with TIP3P water molecules[31] in a 50 Å cubic box and neutralized with Cl^- ions. To obtain the mixed-solvent systems, an appropriate number of water molecules was replaced with GB or TMAO molecules to obtain a 1 M solution. Simulations were run using the GROMACS[32] package combined with the PLUMED[33] plug-in, which implements BEMD. As in other collective variables (CV)-based techniques, biasing the evolution of the system along a few variables approximating the reaction coordinate, the convergence of metadynamics can be severely affected by neglecting slow CVs. The BEMD method complements the

Received: July 8, 2011
Published: September 20, 2011

metadynamics technique introducing a replica exchange algorithm, compensating for this eventual neglect and allowing for a larger number of CVs with respect to standard metadynamics. Albeit BEMD, at difference with the more computationally expensive PTmetaD,[21] might have convergence problems in complex systems, it has already been shown to converge well in the case of HP35 folding.[34] What is more, we have carefully checked the convergence of the free energy profiles reconstructed from the blank replica as a function of simulation time. The Amber99SB*-ILDN[35,36] force field was used, including backbone corrections.[37] Particle-mesh Ewald was used with a cutoff of 0.8 nm. All bond lengths were constrained to equilibrium distances using the LINCS[38] algorithm. After minimization, the systems were relaxed with 1 ns NPT dynamics, at 320 K and 1 atm, using the V-Rescale[39] algorithm for temperature coupling and a Berendsen barostat.[40] The BEMD runs were performed with the same collective variables (CVs) used in ref 34, i.e., the number of backbone hydrogen bonds, salt bridges, and hydrophobic contacts; the correlation of the backbone dihedral angles; and the fraction of secondary structure, and a neutral replica, on which no bias was applied. Each BEMD simulation required considerably longer simulations than those used in ref 34 to converge (>300 ns). This is most probably due to the different version of the Amber force-field used. Analyses were performed on the neutral replica, whose free energy profiles along the CV were reconstructed from the unbiased probability distribution of the states. The free energy of unfolding was calculated by integrating the density of the folded (F) and unfolded (U) states according to

$$\Delta G_{\text{unfold}} = k_B T \log\left(\frac{\int_F ds \exp\left(-\frac{G(s)}{k_B T}\right)}{\int_U ds \exp\left(-\frac{G(s)}{k_B T}\right)}\right) \quad (1)$$

Preferential coefficients (Γ_{XP}) were calculated using the approach developed by Baynes and Trout.[41] According to this approach, Γ_{XP} can be evaluated defining two domains, a bulk domain (I) and a protein domain (II), and calculating

$$\Gamma_{XP} = \left\langle n_X^{II} - n_W^{II}\left(\frac{n_X^I}{n_W^I}\right)\right\rangle \quad (2)$$

where $n_{X,W}^{I,II}$ is the number of water (W) or osmolyte (X) molecules in the I and II domains. The solvent density function (SDF) that describes how the molecules of osmolyte are distributed around the protein is, in principle, equivalent to the radial distribution function but takes into account the shape and volume of the protein. The SDF for a generic molecule X is computed as

$$\rho_X(r) = \frac{X(r,r')}{V(r,r')} \quad (3)$$

where r is the radius of the solvation shell, $X(r,r')$ is the number of X molecules found from rr to r', and $V(r,r')$ is the volume of the shell from r to r'. The number of molecules $X(r,r')$ was obtained calculating n_X^{II} for different r values. The volume $V(r,r')$ was calculated on the basis of the grid-based solvent-accessible methodology of ref 42. Bulk dielectric constants were calculated, according to Neumann's formulation,[43] from the fluctuations of the total dipole moment $\langle M^2\rangle$ following the approach reported in ref 44. Three different systems, comprising only the mixed-solvent, were simulated by standard MD with the same parameters as described before, for a total production phase of 55 ns. The rotational correlation function was calculated using the same systems, following the derivation of Lipari and Szabo for NMR relaxation times[45,46] with a first-order Legendre polynomial. A detailed explanation of the procedure is reported in ref 44 and the references therein.

Human villin headpiece subdomain HP35, LSIED FTQAF GMTPA AFSAL PKWKQ QNLKK EKGLF, was synthesized by Proteogenix (France) with a purity >95%. All CD measurements were performed on a JASCO-810 dichrograph equipped with a Peltier thermoelectric temperature controller. CD spectra of HP35 in water at a concentration of 70 μM were recorded between 190 and 260 nm, with a 0.1-cm-path-length quartz cuvette (Hellma), a 50 nm/min scanning speed, an averaging time of 4 s, and a bandwidth of 1 nm. The spectra shown are the averages of three scans. Thermal denaturation experiments were performed at constant heating rates of 1 °C/min by following the ellipticity at 222 nm from 5 to 90 °C with a total sample concentration of 50 μM. The analysis of the thermal unfolding curve was performed by nonlinear least-squares fitting according to a two-state model.[47] Equilibrium urea denaturation was monitored by CD in the wavelength range of 210−260 nm and at seven different temperatures between 10 and 40 °C. HP35 solutions at a 50 μM concentration were mixed with varying amounts of stock solution containing 8 M urea. Unfolding was monitored in the range of 0−7 M urea. The urea unfolding profile of HP35 is described by the change of the dichroic signal at 222 nm as a function of denaturant concentration. Chemical denaturation data were analyzed by nonlinear least-squares fitting of the observed CD signal $[\theta]_t$ to a two-state model of a single unfolding transition between folded (F) and unfolded (U) states:[48]

$$[\theta]_t = \alpha_i([\theta]_U - [\theta]_F) + [\theta]_F \quad (4)$$

where $[\theta]_F$ is the ellipticity at which the molecule is fully folded and $[\theta]_U$ is the ellipticity of the fully unfolded molecule. The fractional population of the unfolded form (α_i) is determined from the equilibrium constant for unfolding:

$$K_{Ui} = \exp\left(-\frac{\Delta G_i}{RT}\right) \quad (5)$$

where R is the gas constant, which equals 1.98 cal/mol, and T is the absolute temperature. ΔG_i is calculated using the linear extrapolation model (LEM):[49]

$$\Delta G_i = \Delta G_0 - m_{\text{urea}}[\text{urea}] \quad (6)$$

where ΔG_0 is the standard free energy of unfolding in the absence of denaturant and m_{urea} is the slope, which characterizes the change in ΔG_i with [urea]. The denaturant concentration midpoint of the transition, $[\text{urea}]_{(1/2)}$, is equal to $\Delta G_0/m$. The combined effect of urea and the osmolyte TMAO (or GB) on unfolding free energies was modeled as being linear in both cosolvents:[50]

$$\Delta G_i = \Delta G_0 - m_{\text{urea}}[\text{urea}] - m_{\text{osmolyte}}[\text{osmolyte}] \quad (7)$$

Equation 7 was globally fitted to unfolding transitions in mixtures of urea and osmolyte to yield the free energy of unfolding in the absence of both cosolvents. In order to correctly determine the ΔG in the presence of osmolyte, the unfolded fraction was calculated by using the $[\theta]_U$ value derived

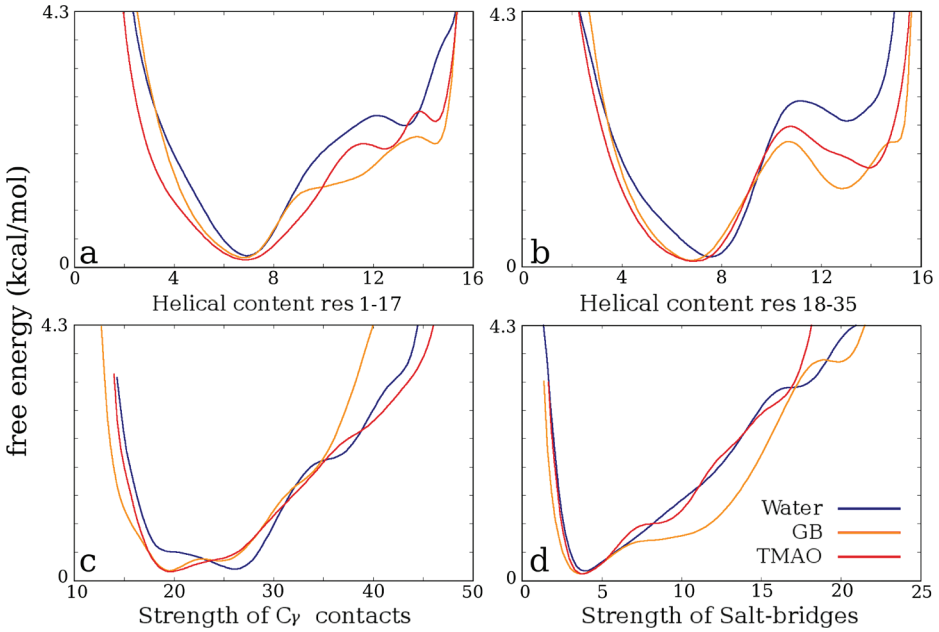

Figure 1. Free energy profile as a function of the helical content of residues 1−17 (a) and residues 18−35 (b) of the protein. Free energy profile as a function of the strength of hydrophobic contacts (c) and the strength of salt bridges (d). When the osmolyte is added to the solution, structures with a higher helical content become more populated as conformations with a higher number of salt bridges and less hydrophobic contacts. See ref 34 for the exact definition of the CVs. The typical error due to the convergence of the free energy profiles is reported in Supporting Information Figure S2.

in the absence of osmolytes with urea.[51] Heat capacity change (ΔC_p) for HP35 unfolding was measured by globally fitting the thermal and chemical denaturation data to the Gibbs−Helmholtz equation:[52]

$$\Delta G(T) = \Delta H_m\left(1 - \frac{T}{T_m}\right) - \Delta C_p\left[(T_m - T) + T\ln\left(\frac{T}{T_m}\right)\right] \quad (8)$$

where $\Delta G(T)$ is ΔG at temperature T, T_m is the midpoint of the thermal unfolding curve, and ΔH_m is the enthalpy change for unfolding measured at T_m.

RESULTS AND DISCUSSION

The availability of high-resolution experiments on HP35 folding enables a careful validation of the computational results.

Here, we use previously reported simulations of HP35 in pure water[53] in good agreement with experiments as a reference for the simulations of the osmolyte solutions: a 1.5-μs-long fully atomistic MD simulation at 298 K starting from the lowest energy NMR structure (PDB code: 1UNC)[22] and massive BEMD simulations at 298 K and 320 K, close to the experimental melting temperature (see the Supporting Information), were used to reconstruct a fully converged free-energy landscape of HP35 folding. We used the recently described Amber99SB*-ILDN[35] force field, including several improvements.[36,37]

We repeated the BEMD simulations in the presence of 1 M GB, 1 M TMAO, and, for comparison, 1 M urea, a denaturant. The folded minimum in water (Figure 1) is, in every case, narrow and centered around the values typical of the native structure. The minima in osmolyte solutions are generally broader, and it can be seen (Figure 1c,d) that the osmolytes weaken the hydrophobic core and strengthen the salt bridges. The weakening of the hydrophobic core corresponds to a slight increase of the exposed surface in the folded state and a more sizable increase in the unfolded ensemble, leading to a ΔSASA in good agreement with the observed increase of the heat capacity ΔC_p (see Supporting Information Table S1). The protein in osmolyte solutions adopts more helical conformations, as can be seen from the free energy profiles (Figure 1a,b) showing lower minima at higher helical values (∼14). Since the typical value for the native state is ∼8, the higher helical content is found mainly in the unfolded ensemble. From 2D FES (Figure S1, Supporting Information), it is clear that the N and N′ free energy basins observed in the pure water simulations[53] are merged in the presence of the osmolytes and that HP35 is more flexible. Another alternative explanation is that the N′ state becomes the most stable native structure over the more rigid N state.

As expected, the free energy profiles of HP35 in urea are significantly different. The FE profiles (Figure S3, Supporting Information) show a narrower minimum corresponding to the folded state, while cluster analysis of the main structures indicates that in urea a partial disruption of the hydrophobic core takes place, with a strong destabilization of helix 3, in contrast to the effect observed for the stabilizing osmolytes. Using 3D FES (Figure S4 and S5, Supporting Information), the unfolding free energy (ΔG_{unfold}) was calculated by integrating the densities of the folded and unfolded states. The resulting values are −0.04 kcal/mol for the simulation in water, 0.61 and 0.69 kcal/mol, respectively, for 1 M GB and TMAO (Table 1), and −0.5 kcal/mol for urea. As expected, the ΔG_{unfold} is lower for the urea solution, since unfolding is favored with respect to water, and positive for the two protecting osmolytes.

In order to assess whether or not GB and TMAO engage in direct interactions with the protein backbone, we analyzed the distribution of osmolyte molecules around the protein. Calculating the solvent density function (SDF) for GB and TMAO molecules, no relevant peak was observed, suggesting the

Table 1. Thermodynamic Parameters for HP 35 in Pure Water and in NaCl or Osmolite Solutions[a]

	ΔH	ΔC_p	T_m	$\Delta G_{47°C}{}^{b}$	$\Delta\Delta G_{47°C}$	$\Delta G_{47°C}^{calcd\,c}$	$\Delta\Delta G_{47°C}^{calcd}$
H_2O	24.8 ± 0.9	0.37 ± 0.06	44 ± 0.1	−0.24		−0.04	
NaCl 0.66 M	26.7 ± 0.8	0.44 ± 0.05	49 ± 0.1	0.16	0.40	0.69	0.73
GB 1 M	30.7 ± 3.7	0.72 ± 0.22	49 ± 0.1	0.19	0.43	0.61	0.65
TMAO 1 M	33.4 ± 1.5	0.96 ± 0.09	51 ± 0.1	0.39	0.63	0.69	0.73

[a] Values are in kcal mol^{-1} for ΔH, kcal mol^{-1} K^{-1} for ΔC_p, °C for T_m, and kcal mol^{-1} for ΔG. [b] Obtained from the experiments employing the Gibbs−Helmholtz equation. [c] Obtained from the calculated free energy surfaces.

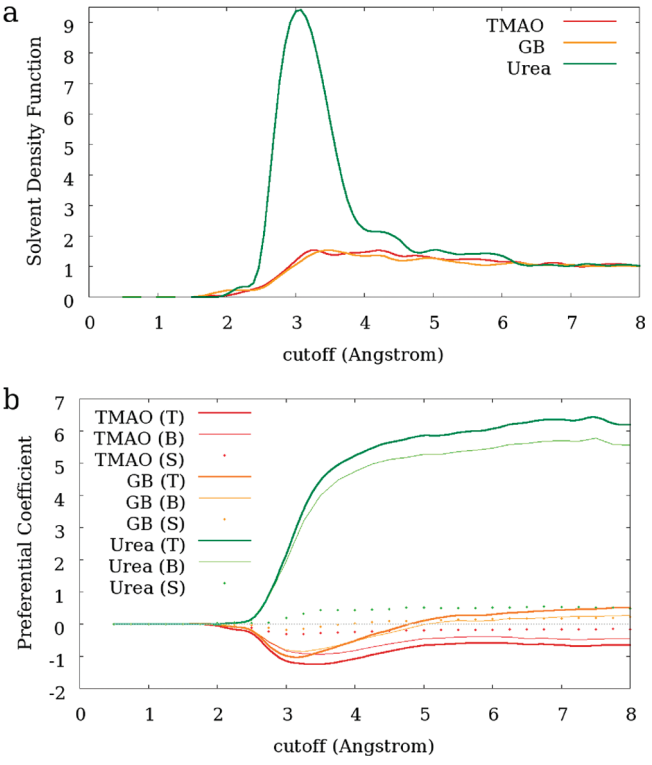

Figure 2. (a) Solvent density function for GB, TMAO, and urea. Only a very slight increase with respect to the bulk limit is observable for the osmolytes with a preferred distance of 3.8 Å. The absence of a well-defined prominent peak suggests that GB and TMAO are excluded from the protein surface, as demonstrated experimentally. The typical 2.8 Å peak is clearly recognizable for urea, confirming its proximity to the protein surface. (b) Preferential coefficient for HP35 in 1 M solutions of GB, TMAO, and urea: total (T), side chain contribution (S), and backbone contribution (B). The negative values in the region 3−5 Å clearly show a preference of the two osmolytes for the bulk domain.

absence of direct contacts between the osmolytes and the protein (Figure 2a), in agreement with refs 16 and 20. The preferential coefficient Γ_{XP} is calculated to confirm the proposed osmophobic effect[16,19] (see Figure 2b). Choosing a cutoff of 4 Å for the boundary between protein and bulk domains, we obtained a value of −0.52 for GB and −1.08 for TMAO, in agreement with the suggested osmophobic effect. As a comparison, the corresponding value for HP35 in 1 M urea solution is 5.22, confirming urea contacts with the protein.[54] For all molecules, the most relevant contribution to Γ_{XP} came from the backbone, in agreement with previous results.[55]

The observed differences in the FE profiles due to the osmolytes and the lack of direct interactions with the protein are in agreement with the "indirect" hypothesis. This, together with the proposed changes in the water structure[16,56] due to the osmolytes, led us to investigate whether or not a shift of the dielectric constant would explain the protecting effects. An increase of the ε value was reported for several osmolytes, including TMAO, GB, taurine, and sarcosine.[57,58] We calculated the static dielectric constant ε according to Neumann's formulation,[43,44] obtaining a value of 98.0 (±0.2) for TIP3P water and significantly higher values for the 1 M osmolyte solutions: 106.4 (±0.2) for GB and 103.0 (±0.2) for TMAO, in agreement with the experiments. For comparison, the ε for the 1 M urea solution was 95.2 (±0.2), similar to that of pure water. These results, suggesting an increased polarity of the solution, are not consistent with the observed increase of salt bridges and hydrophobic core relaxation. However, when we examined more in detail the properties of the solution in the previously defined protein domain, we found a possible explanation to the discrepancy. Osmolytes also affect the rotational dynamics of water molecules both in the bulk and in the protein domain. Indeed, the rotational diffusion is significantly reduced, as shown by the calculated rotational correlation function, showing higher correlation times for water molecules in both 1 M GB and TMAO (Figure 3).

Thus, the high dipole moment of the osmolyte molecules has two different effects on the solution: on the one hand, it causes a considerable increase in the overall dielectric constant; on the other hand, it tends to align the water dipoles. Since, as we have seen the osmolytes are excluded from the protein surface, the lower rotational diffiusion of water in the protein first solvation shells has the effect of reducing the local ε of the solution. The calculated ε around the protein is significantly smaller, even compared to that of pure water, 83.0 for GB and 90.3 for TMAO.

These results are in agreement with both NMR[59] and IR[60] observations. ^{1}H NMR data[59] demonstrate a decrease of T_1 relaxation time (i.e., an increase of the rotational correlation time τ_C[61]) for several osmolytes, including TMAO, GB, sarcosine, sorbitol, and trehalose. Lower T_1 relaxation times have been ascribed to a more "ice-like" behavior of water (it is to be noted that the ε_0 of ice is 3.19[62]), confirmed by the shifts in NIR spectra.[59] Very recently a similar observation was obtained by 2D infrared spectroscopy on TMAO solutions.[60] Bakulin and coworkers demonstrate the slower rotational reorientation of water molecules around TMAO molecules, supporting the results of our calculations. Much slighter variations, occasionally in the same direction of those observed for protecting osmolytes, are registered for urea, suggesting that the source of the different effect of urea resides mainly in its interactions with the protein. Most of the reported features of osmolyte behavior (e.g., folded state protection, osmophobic effect and backbone repulsion) can be solidly explained in the context of an "ice-like" shift in the aqueous solvent dynamical behavior, due to GB or TMAO addition. The slowing down of water rotational diffusion is highly

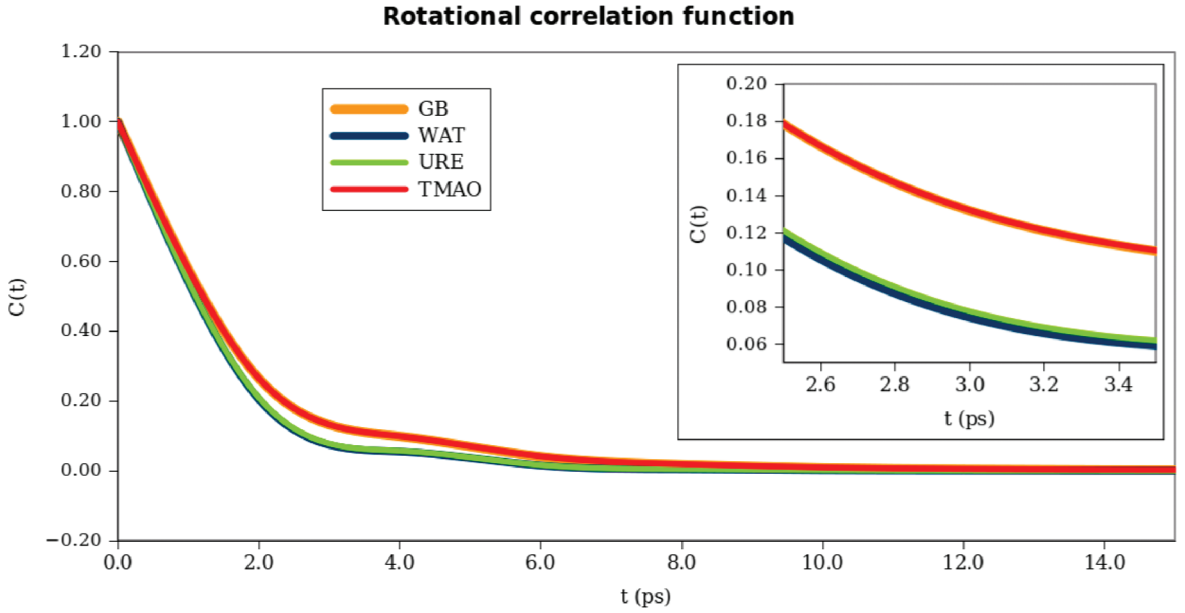

Figure 3. Rotational correlation function for the simulated systems: pure water and 1 M solutions of TMAO, GB, and urea. An increase of the rotational correlation time can be observed for the two protecting osmolytes.

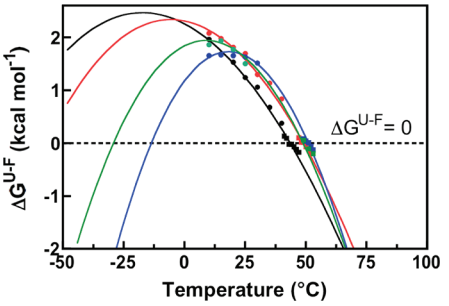

Figure 4. Protein stability curves for HP35 in water (black), 0.66 M NaCl (red), 1 M GB (green), or 1 M TMAO (blue). Squares represent unfolding free energies measured directly from the transition zones of the thermal denaturation curves shown in Figure 2 at an HP 35 concentration of 50 μM. Circles represent $\Delta G_U^{H_2O}$ values determined from an analysis of urea denaturation curves determined at various temperatures. Solid lines show the best fit to the Gibbs−Helmholtz equation.

consistent with previous hypotheses describing the osmolytes effect as a "water-structuring" effect.[63,64] The water molecules' rotational diffusion slowdown is perceived as an average effect by the protein itself, and the change in water rotational properties affects the thermodynamic and electrostatic response properties of the solvent.

To confirm this new formulation of the "indirect hypothesis", we performed a BEMD simulation of HP35 in modified TIP3P water molecules (W79), whose charges were scaled down to reproduce the decreased dielectric constant of water in the 1 M GB solution. The FE profiles were strikingly similar to those obtained for the osmolyte solutions (Figure S6 and S7, Supporting Information). Cluster analysis revealed a high similarity of the most populated conformers in 1 M GB and W79, with a RMSD within 2.1 Å; the salt bridge previously observed in 1 M GB was also observed in W79 (Figure S8, Supporting Information). Hence, the W79 simulation provided further evidence that a dielectric constant shift (i.e., a rotational diffusion slowdown) in the protein domain can explain most of the features of the osmolyte solution.[16]

To validate computational results, we exploited thermal and chemical denaturation to gain an in-depth thermodynamic description of the effects due to the osmolytes. Equilibrium thermal unfolding measurements were performed on HP35 in water and in 1 M TMAO or GB solutions. The stability was also investigated in a 0.66 M NaCl solution. This salt concentration reduces the dielectric constant to 67.2,[65] similar to the shift observed for water in a 1 M GB solution. HP35 showed a cooperative, sigmoidal transition (Supporting Information Figure S9), and the data fit a two-state model. HP35 in water shows a transition temperature (T_m) of 44 °C. TMAO or GB increases the T_m to 51 and 49 °C, respectively. Similarly, HP35 in 0.66 M NaCl unfolds with a T_m of 49 °C. At 25 °C, the midpoint of the urea-induced chemical denaturation is 2.9 M in water, 3.6 M in NaCl, and 3.5 M in GB or TMAO. These results indicate a clear stabilization of the native state and are in excellent agreement with the predictions of the simulations. The unfolding reaction of HP35 showed similar m values in all solutions, suggesting similar cooperativity (Supporting Information Table S2). One explanation is that osmolytes are not directly in contact with the protein backbone, in agreement with the results of the simulations. Consistent with this, proton NMR cross-relaxation (ROESY) experiments were unable to detect any TMAO-HP35 contact (see Supporting Information Figures S12 and S13), indicating the absence of direct and persistent (ms time scale) interactions between osmolyte and protein. From the combination of thermal and chemical denaturation, we obtained the stability plot of HP35 and calculated the unfolding ΔG. It is evident (Figure 4 and Table 1) that the osmolytes determine an increase of stability with respect to pure water, in agreement with the calculated values.

CONCLUSIONS

The pursuit of a universal explanation for the osmoprotectant effect has drawn considerable attention in recent decades, due to

its significant importance for both fundamental and applied science. In recent years, the studies of Bolen and coworkers[11,19,55] have succeeded in the defining a simplified model, based on transfer free energies, with considerable predictive power. However, despite multiple efforts and ever increasing interest, a simple yet general microscopic explanation of the mechanism underlying osmolyte-mediated protein protection mainly remains an open issue. State-of-the-art in silico simulations and experiments allowed us to make a significant step forward toward this goal. Our results support a new flavor of the previously reported "indirect hypothesis" and put forward a very simple explanation: the main driving force behind native state protection is a slowdown of the solvent rotational dynamics. The "slower" solvent behaves around the protein, where the osmolytes are excluded, as a colder or lower dielectric aqueous solvent. This local reduction is consistent with, and explanatory of, all reported theoretical and experimental results.[11,16,19,55] Indeed, the alteration of the solvent is translated into a decreased denaturing power of the water molecules that, acting as a less polar media with the dynamical behavior of a lower temperature solvent, is less effective in interfering with the intraprotein interactions sustaining the native fold. This, in turn, explains not only the osmoprotecting effect and the increase of the melting temperature of proteins but also the significant role of backbone interactions, whose importance was systematically predicted by transfer models.

■ ASSOCIATED CONTENT

Supporting Information. Additional free energy profiles of HP35 in water and in 1 M solutions, 2D and 3D free energy maps, CD and NMR spectra, and thermal denaturation curves. This information is available free of charge via the Internet at http://pubs.acs.org/.

■ AUTHOR INFORMATION

Corresponding Author
*E-mail: maurizio.sironi@unimi.it; flgervasio@cnio.es.

■ ACKNOWLEDGMENT

We acknowledge support by the Spanish Science and Innovation (MICINN) grant (BIO2010-20166, "AlteredDynamics"). M. Morando is acknowledged for helpful discussions. G.S. acknowledges the European Commission Capacities Area—Research Infrastructures Initiative HPC-EUROPA2 (project number: 228398) for partial support. The Barcelona Supercomputing Center is acknowledged for a generous allocation of computer resources.

■ REFERENCES

(1) Yancey, P. H.; Clark, M. E.; Hand, S. C.; Bowlus, R. D.; Somero, G. N. *Science* **1982**, *217*, 1214–1222.
(2) Yancey, P. H.; Burg, M. B. *Am. J. Physiol.* **1989**, *257*, 602–607.
(3) Yancey, P. H. *J. Exp. Biol.* **2005**, *208*, 2819–30.
(4) Weber, D. J. *Salinity and Water Stress*; Springer Netherlands: Dordrecht, The Netherlands, 2009; Vol. 44, p 236.
(5) Furini, A.; Koncz, C.; Salamini, F.; Bartels, D. *EMBO J.* **1997**, *16*, 3599–3608.
(6) Baldwin, W. W.; Myer, R.; Kung, T.; Anderson, E.; Koch, A. L. *J. Bacteriol.* **1995**, *177*, 235–237.
(7) Cayley, S.; Lewis, B. A.; Guttman, H. J.; Record, M. T.; et al. *J. Mol. Biol.* **1991**, *222*, 281–300.
(8) Csonka, L. N. *Microbiol. Rev.* **1989**, *53*, 121–147.
(9) Hochachka, P. W.; Somero, G. N. *Biochemical adaptation: mechanism and process in physiological evolution*; Oxford University Press: New York, 2002; p 466.
(10) Qu, Y.; Bolen, C. L.; Bolen, D. W. *Proc. Natl. Acad. Sci. U.S.A.* **1998**, *95*, 9268–73.
(11) Baskakov, I. V.; Bolen, D. W. *J. Biol. Chem.* **1998**, *273*, 4831–4834.
(12) Moriyama, T.; Garcia-Perez, A.; Olson, A. D.; Burg, M. B. *Am. J. Physiol.* **1991**, *260*, 494–497.
(13) Burg, M. B.; Ferraris, J. D. *J. Biol. Chem.* **2008**, *283*, 7309–13.
(14) Xie, G.; Timasheff, S. N. *Biophys. Chem.* **1997**, *64*, 25–43.
(15) Street, T. O.; Bolen, D. W.; Rose, G. D. *Proc. Natl. Acad. Sci. U.S.A.* **2006**, *103*, 13997–14002.
(16) Zou, Q.; Bennion, B.; Daggett, V.; Murphy, K. *J. Am. Chem. Soc.* **2002**, *124*, 1192–1202.
(17) Wang, A.; Bolen, D. W. *Biophys. J.* **1996**, *71*, 2117–2122.
(18) Canchi, D.; Paschek, D.; García, A. *J. Am. Chem. Soc.* **2010**, *132*, 2338–2344.
(19) Bolen, D. W.; Baskakov, I. V. *J. Mol. Biol.* **2001**, *310*, 955–63.
(20) Saladino, G.; Pieraccini, S.; Rendine, S.; Recca, T.; Francescato, P.; Speranza, G.; Sironi, M. *J. Am. Chem. Soc.* **2011**, *133*, 2897–2903.
(21) Bussi, G.; Gervasio, F. L.; Laio, A.; Parrinello, M. *J. Am. Chem. Soc.* **2006**, *128*, 13435.
(22) Vermeulen, W.; Vanhaesebrouck, P.; Troys, M. V.; Verschueren, M.; Fant, F.; Goethals, M.; Ampe, C.; Martins, J. C.; Borremans, F. A. M. *Protein Sci.* **2004**, *13*, 1276–1287.
(23) McKnight, C. J.; Doering, D. S.; Matsudaira, P. T.; Kim, P. S. *J. Mol. Biol.* **1996**, *260*, 126–34.
(24) Duan, Y.; Kollman, P. A. *Science* **1998**, *282*, 740.
(25) Zagrovic, B.; Snow, C. D.; Shirts, M. R.; Pande, V. S. *J. Mol. Biol.* **2002**, *323*, 927–937.
(26) Frank, B. S.; Vardar, D.; Buckley, D. A.; McKnight, C. J. *Protein Sci.* **2002**, *11*, 680–7.
(27) Kubelka, J.; Henry, E. R.; Cellmer, T.; Hofrichter, J.; Eaton, W. A. *Proc. Natl. Acad. Sci. U.S.A.* **2008**, *105*, 18655–62.
(28) Tang, Y.; Rigotti, D.; Fairman, R.; Raleigh, D. *Biochemistry* **2004**, *43*, 3264–3272.
(29) Havlin, R. H.; Tycko, R. *Proc. Natl. Acad. Sci. U.S.A.* **2005**, *102*, 3284–9.
(30) Piana, S.; Laio, A. *J. Phys. Chem. B* **2007**, *111*, 4553–4559.
(31) Jorgensen, W. L. *J. Am. Chem. Soc.* **1981**, *103*, 335–340.
(32) Hess, B.; Kutzner, C.; Spoel, D. V. D.; Lindahl, E. *J. Chem. Theory Comput.* **2008**, *4*, 435–447.
(33) Bonomi, M.; Branduardi, D.; Bussi, G.; Camilloni, C.; Provasi, D.; Raiteri, P.; Donadio, D.; Marinelli, F.; Pietrucci, F.; Broglia, R. A.; et al. *Comput. Phys. Commun.* **2009**, *180*, 1961–1972.
(34) Piana, S.; Laio, A.; Marinelli, F.; Troys, M. V.; Bourry, D.; Ampe, C.; Martins, J. C. *J. Mol. Biol.* **2008**, 460–470.
(35) Hornak, V.; Abel, R.; Okur, A.; Strockbine, B.; Roitberg, A.; Simmerling, C. *Proteins: Struct. Funct. Bioinf.* **2006**, *65*, 712–725.
(36) Lindorff-Larsen, K.; Piana, S.; Palmo, K.; Maragakis, P.; Klepeis, J. L.; Dror, R. O.; Shaw, D. E. *Proteins: Struct. Funct. Bioinf.* **2010**, *78*, 1950–8.
(37) Best, R. B.; Buchete, N. V.; Hummer, G. *Biophys. J.* **2008**, *95*, L07–L09.
(38) Hess, B.; Bekker, H.; Berendsen, H. J.; Fraaije, J. G. *J. Comput. Chem.* **1997**, *18*, 1463–1472.
(39) Bussi, G.; Donadio, D.; Parrinello, M. *J. Chem. Phys.* **2007**, *126*, 014101.
(40) Berendsen, H. J. C.; Postma, J. P. M.; Gunsteren, W. F. V.; DiNola, A.; Haak, J. R. *J. Chem. Phys.* **1984**, *81*, 3684.
(41) Baynes, B. M.; Trout, B. L. *J. Phys. Chem. B* **2003**, *107*, 14058–14067.
(42) Beck, D. A.; Alonso, D. O.; Daggett, V. *Biophys. Chem.* **2003**, *100*, 221–237.

(43) Neumann, M. *J. Chem. Phys.* **1985**, *82*, 5663–5672.
(44) van der Spoel, D.; Maaren, P. J. V.; Berendsen, H. J. *J. Chem. Phys.* **1998**, *108*, 10220–10230.
(45) Lipari, G.; Szabo, A. *J. Am. Chem. Soc.* **1982**, *104*, 4559–4570.
(46) Lipari, G.; Szabo, A. *J. Am. Chem. Soc.* **1982**, *104*, 4546–4559.
(47) Greenfield, N. J. *Nat. Protoc.* **2007**, *1*, 2527–2535.
(48) Greenfield, N. J. *Nat. Protoc.* **2006**, *1*, 2733–2741.
(49) Myers, J.; Pace, C.; Scholtz, J. *Protein Sci.* **1995**, *4*, 2138–2148.
(50) Mello, C.; Barrick, D. *Protein Sci.* **2003**, *12*, 1522–1529.
(51) Wu, P.; Bolen, D. *Proteins: Struct. Funct. Bioinf.* **2006**, *63*, 290–296.
(52) Pace, C.; Laurents, D. *Biochemistry* **1989**, *28*, 2520–2525.
(53) Saladino, G.; Marenchino, M.; Gervasio, F. L. *J. Chem. Theory Comput.* **2011**, *7*, 2675–2680.
(54) Stumpe, M. C.; Grubmüller, H. *PLoS Comput. Biol.* **2008**, *4*, e1000221.
(55) Street, T.; Bolen, D.; Rose, G. *Proc. Natl. Acad. Sci. U.S.A.* **2006**, *103*, 13997–14002.
(56) Niebuhr, M.; Koch, M. H. *Biophys. J.* **2005**, *89*, 1978–1983.
(57) Shikata, T.; Itatani, S. *J. Sol. Chem.* **2002**, *31*, 823–844.
(58) Wyman, J. *Chem. Rev.* **1936**, 213–239.
(59) Lever, M.; Blunt, J. W.; Maclagan, R. G. *Comp. Biochem. Physiol.* **2001**, *130*, 471–86.
(60) Bakulin, A. a.; Pshenichnikov, M. S.; Bakker, H. J.; Petersen, C. *J. Phys. Chem. A* **2011**, *115*, 1821–9.
(61) Yoshida, K.; Ibuki, K.; Ueno, M. *J. Chem. Phys.* **1998**, *108*, 1360.
(62) Mätzler, C.; Wegmüller, U. *J. Phys. D* **1988**, *21*, 1660–1660.
(63) Bennion, B. J.; Daggett, V. *Proc. Natl. Acad. Sci. U.S.A.* **2003**, *100*, 5142.
(64) Bennion, B.; Daggett, V. *Proc. Natl. Acad. Sci. U.S.A.* **2004**, *101*, 6433.
(65) Haggis, G. H.; Hasted, J. B.; Buchanan, T. J. *J. Chem. Phys.* **1952**, *20*, 1452–1465.